Talanta 230 (2021) 122314

Contents lists available at ScienceDirect

Talanta

journal homepage: www.elsevier.com/locate/talanta

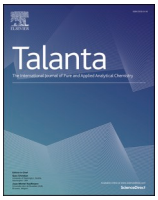

Multiphoton Excitation Fluorescence Microscopy and Spectroscopic Multianalytical Approach for Characterization of Historical Glass Grisailles

M. Oujja [a,*], F. Agua [b], M. Sanz [a,c], D. Morales-Martin [b], M. García-Heras [b], M.A. Villegas [b], M. Castillejo [a]

[a] Instituto de Química Física Rocasolano (CSIC), C/ Serrano 119, 28006, Madrid, Spain
[b] Instituto de Historia (CSIC), C/ Albasanz 26-28, 28037, Madrid, Spain
[c] Departamento de Física Interdisciplinar, Facultad de Ciencias, Universidad Nacional de Educación a Distancia (UNED), Senda Del Rey 9, 28040, Madrid, Spain

ARTICLE INFO

Keywords:
Nonlinear optical microscopy
Multi-photon excitation fluorescence
Laser spectroscopies
Historical stained glasses
Grisaille paint layers

ABSTRACT

The preservation of the integrity of artworks and cultural heritage items during characterization and conservation operations is of high priority, therefore, the application of non-invasive techniques is commonly suggested and recommended. Nonlinear optical microscopies (NLOM), based on the use of tightly focused pulsed femtosecond lasers, are emerging techniques for structural and chemical analysis of heritage objects with micrometric lateral and axial resolution. The results obtained with a set of optical and spectroscopic techniques for the chemical and physical characterization of grisaille paint layers on historical stained glasses, from different chronologies and provenance in Spain, are presented in this work. Optical behaviour and chemical composition were investigated by NLOM, using a laboratory set-up in the modality of Multi-Photon Excitation Fluorescence (MPEF), and by a multi-analytical combination of Field Emission Scanning Electron Microscopy-Energy Dispersive X-ray Spectrometry (FESEM-EDS), Laser Induced Breakdown Spectrosocopy (LIBS) and Laser Induced Fluorescence (LIF). Thicknesses values of the historical grisaille paint layers measured with MPEF were compared with those retrieved through FESEM, showing significant consistency and agreement. Under proper conditions, analysis via MPEF microscopy avoids the photochemical and physical damage to the examined materials, thus ensuring their preservation. This approach paves the way for future in-situ, non-invasive stratigraphic investigations on cultural heritage objects.

1. Introduction

Stained glass windows are one of the most impressive features of medieval Gothic architecture in Western Europe [1,2]. From the 12th century [3–5], their use spread with the construction of the largest cathedrals, in response to the increasing size of the windows of these buildings, which serve as iconographic supports and fill medieval churches with light and color.

Grisailles and vitrifiable paints applied on glass have been used since medieval times to make decorations and symbolic representations in stained glass. A grisaille is a blackish-brown paint that is most often applied on the inside surface of a stained-glass window to draw the contours and details of figures (with a thick line) and to produce the effect of shadows and volumes (with a thin layer). The thickness of a grisaille is indicative of the kind of design applied, i.e. whether such grisaille can be considered as contour or as shadow in the decoration. In terms of artistic meaning this is very relevant for restorers and art historians as it allows them to compare with existing documents on artistic and iconographic information about the whole stained-glass window. In turn, such information connects with specific chronological and artistic styles and procedures of glass painting. Grisaille production involves mixing finely ground iron oxides, but also copper, zinc, lead or manganese mixed with a flux such as lead ground glass ($PbO–SiO_2$) [6–8]. Other common components for the preparation of grisailles are linseed oil, fish oil or gum arabic, which serve as agent/vehicle for its application on glass pieces. After firing at 650–700 °C, a thin layer of a glassy matrix is obtained with embedded dark metal oxides.

Even though most glasses are well resistant against natural deterioration, with the exception of potash lime silicate glasses and other glasses subjected to aggressive treatments and/or environments (e.g. polluted air, under sea water), glass deterioration should not be discarded in ancient and historical items made of glass or containing glass

* Corresponding author.
E-mail address: m.oujja@iqfr.csic.es (M. Oujja).

https://doi.org/10.1016/j.talanta.2021.122314
Received 17 January 2021; Received in revised form 10 March 2021; Accepted 12 March 2021
Available online 17 March 2021

elements [1,2,9–11]. Decorated and painted glass, associated with pictorial scenes and figures found in church windows, often presents serious preservation challenges [12]. The level of cleaning, repair or protection depends on the chemical composition, condition, quality and importance of the glass. Repairs made hastily, overly aggressive or poorly executed can cause more harm than prolonged deterioration. Therefore, repairs should only be made after careful evaluation, analysis and assessment of the condition of the glass. This task can be accomplished using different types of methodologies based on invasive and non-invasive techniques.

In what regards glass grisailles, its degradation is affected by both its own composition and characteristics and by the type and conservation state of the underlying glass. Many studies on historical glass grisailles have been carried out by some of the present authors (see for instance Refs. [1,2,9]) pointing out to the remarkable interaction between the grisaille layer and the corresponding glass. Several compounds generated during the bulk glass degradation may migrate to the surface reaching the grisaille layer. Depending on the densification degree of the grisaille, such compounds could be accumulated and even react with grisaille components. In the worst case of poorly densified grisailles, the interface glass-grisaille is a free area for deposition of degradation products. This favor the detachment of the grisaille, since its adherence is diminished due to the enlargement of the layer thickness. Environmental temperature fluctuations can also produce cracking, flaking, and detachments due to the different dilatation coefficient between the grisaille and the subjacent glass. This difference in temperature, together with the different dilatation coefficient, can induce mechanical tensions that accelerate formation and development of fissures.

Opacifying elements and chromophores contribute to the chemical composition of the glass in variable proportions since their percentage is often considered as a minor or even a trace component. Common laboratory techniques used to characterize historical glass, such as field emission scanning electron microscopy/energy dispersive X-ray spectroscopy (FESEM/EDS) and conventional X-ray fluorescence spectrometry (XRF), are often destructive, since sampling is necessary and the removed material must be crushed for analysis [13]. These thechniques cannot be applied to whole objects and samples of considerable or relatively large size from museum collections, or to glass items that must be reintegrated into a work of art, such as for example, stained glass windows. However, portable XRF instruments are becoming more and more available for in-situ measurements with the disadvantage that analysis can be only undertaken very near to the glass surface (low penetration). Therefore, the real bulk glass composition cannot be properly determined.

Certainly, the study of valuable historical glasses benefits from the availability of non-invasive or micro-invasive techniques, including 3D structural characterization techniques able to tackle multi-layer and multicomponent structures [14–18]. With the above characteristics, laser spectroscopic techniques including laser-induced breakdown spectroscopy (LIBS) and laser-induced fluorescence (LIF), have been combined in several studies to provide complementary elemental and molecular composition [19–25]. LIBS is a micro-invasive analytical technique based on the spectral analysis of the luminous plume generated by pulsed laser ablation of a small amount of material from the surface of the sample and has the capacity for qualitative, semi-quantitative and quantitative determinations [23–27]. LIBS has shown to be an effective technique for characterization of glasses from a wide variety of perspectives [25,28–34]. Among others, some works have focused on finding the optimal LIBS parameters for the analysis of model soda lime silicate [28] and historical lead silicate glasses [29], on the characterization of chromophores and opacifiers of ancient glasses, and on degradation pathologies [30–32]. On a complementary perspective, LIF spectroscopy provides analytical information and facilitates the detection of trace elements and/or chromophores responsible of the glass coloration in a totally non-invasive way [25,35–42].

Nonlinear optical microscopies (NLOM) are a new set of imaging techniques based on the use of femtosecond lasers recently introduced in the analysis of cultural heritage [43–47]. Various modalities of NLOM, such as Multi-Photon Excitation Fluorescence (MPEF) and Second and Third Harmonic Generation (SHG and THG), account for state-of-the-art non-invasive analysis based on nonlinear optical processes, involving the simultaneous interaction with two or more photons from the laser excitation source with the material of the sample. Femtosecond lasers are used for the excitation of multiphoton signals due to their high peak power and short time duration that favor non-linear optical processes without unwanted side effects such as photobleaching and/or phototoxicity damage. NLOM techniques [43,44,48,49] provide 3D compositional and structural information based on the detection of fluorophores (by MPEF) [43], of crystalline or highly organized structures without inversion symmetry (by SHG) [49] and the position of the boundaries of layers, by virtue of the local differences in the refractive index and third-order nonlinear susceptibility and dispersion (by THG) [18,50]. Despite the proven benifits of NLOM for 3D imaging of cultural heritage substrates and their associated ageing or degradation phenomena, no attempts have been made, to the best of the authors' knowledge, to characterize historic glass using these techniques.

Structural and chemical analysis of a set of stained-glass windows with grisaille paint layers from different historical periods and sites in Spain are presented in this study to understand the possibilities of NLOM in the modality of MPEF to non-invasively characterize these objects. LIF spectra were acquired on the base glasses and on the grisaille paints upon excitation at 266 nm (where the photon energy equals that of 3 photons of the femtosecond infrared excitation wavelength of 800 nm) to determine the emission spectral range and thus allowing to define the spectral acquisition conditions to be used for NLOM analysis via MPEF. To validate the measurements of the grisaille paint layer thicknesses made by MPFE, results obtained by this technique were compared with those retrieved by FESEM on sample cross sections. Finally, EDS and LIBS allow thje identification of chemical elements present in both base glass and grisaille paint layers. While the former is a destructive technique that involves microscopic analysis on cross-sectional small samples, the latter is micro-destructive, does not require sample preparation (analysis is done on the entire historical stained glasses) and allows to carry out analysis in-situ with portable instruments. This multi-analytical study illustrates the possibilities of laser-based microscopies and spectroscopies that do not require sample removal for structural and chemical characterization of heritage objects.

2. Materials and methods

2.1. Samples and historical background

This work undertakes the study of four representative samples of historical stained-glass windows with grisaille paint decorations that come from different Spanish sites and chronology, encompassing a wide period from the 13th to the 20th century. This selection was made considering mainly chronology (from the Middle Ages to the present), grisaille thickness (taking examples of different thicknesses, from about 20 up to 80 μm), characteristics of the grisailles (color, texture, contour or shadow), and availability of samples from previous conservation works made by some of the authors [1,51,52]. Finally, the selection also attended the purpose of studying the largest possible variety of grisaille paints.

The samples, named Balmaseda, Girona, León and Goyeneche according to their place of origin, are glass fragments without value for their replacement; images are shown in Fig. 1 while Table 1 summarizes their relavant details. As it is appreciated in the images, the glasses are decorated with grisailles, either for contour or for shadow, and display different colorations and textures.

The first sample comes from the church of San Severino at Balmaseda, Biscay. Although with some Baroque elements added in the 18th century, this is a Gothic church mainly built in the 15th century.

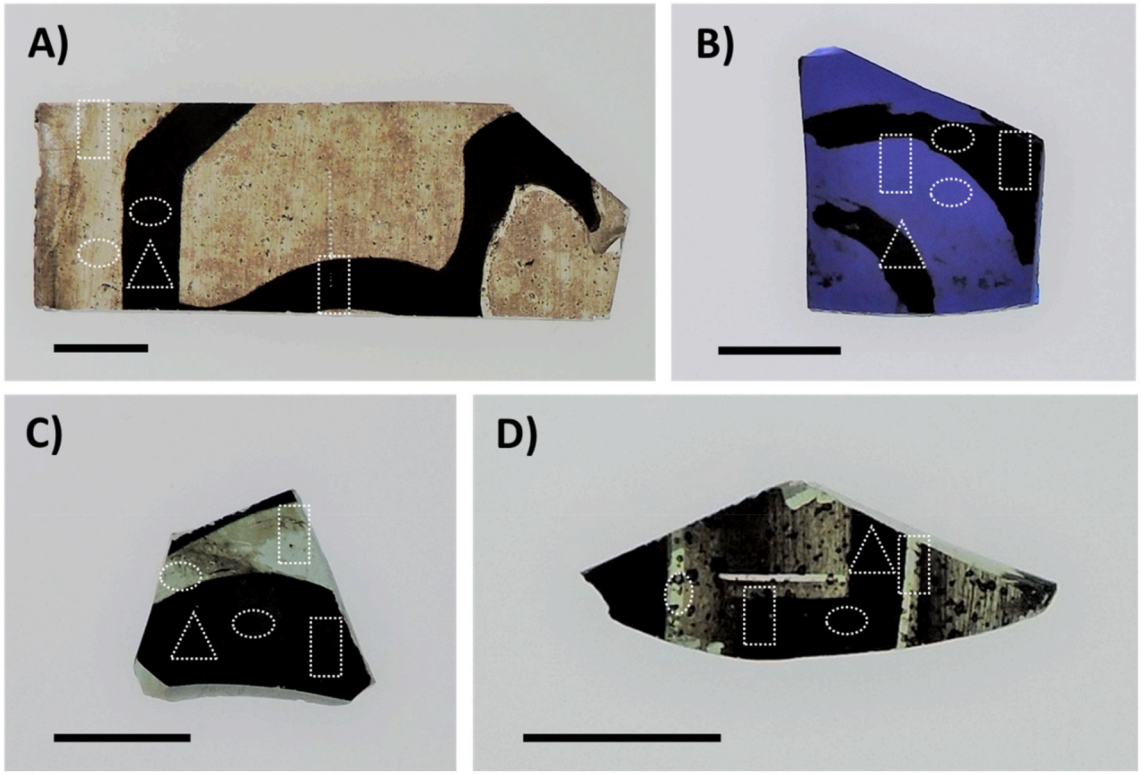

Fig. 1. Glass samples decorated with grisaille paint layers from different sites in Spain: A) Balmaseda, B) Girona, C) León and D) Goyeneche, Madrid. The length of the measurement bars is 1 cm for all images. The areas where LIBS, LIF and MPEF measurements were carried out are indicated by rectangles, circles and triangles, respectively.

Table 1
Description of the studied historical glass samples with grisaille paint layers.

Sample	Origin	Chronology	Characteristics
Balmaseda	Church of San Severino, Balmaseda, Biscay	19th century	Colourless glass with restored black brown grisaille
Girona	West rose window, cathedral of Girona	18th century	Blue glass with black grisaille
León	Cathedral of León	13th century	Green-bluish glass with black grisaille
Goyeneche	Goyeneche House, Madrid	Early 20th century	Green-yellowish glass with black grisaille

However, its stained-glass windows located in the central nave were made in the late 19th century by the French workshop of P. Dagrand. The samples were taken during the restoration and conservation works carried out in 2006.

The second sample is from the cathedral of Girona and comes from the rose window of the west façade. The construction of this cathedral began in the 11th century although was not finished until the 18th century. The stained glasses of the rose window were made in 1732 and the rose is one of the largest Baroque opening windows conserved in Spain. The glass sample was taken during the conservation works accomplished in 2001 [51].

The third sample is the most ancient of those studied here and comes from the Gothic cathedral of León, which was built between the end of the 13th century and throughout all the 14th century. It houses one of the most important set of Gothic stained-glass windows in Europe. The sample comes from one of the low opening windows on the North side of the central nave and was taken during the conservation works carried out in 2004 and 2005 [52].

Finally, the fourth sample comes from the Goyeneche House located in Madrid, which was built in 1915 and decorated with stained glass windows from the Maumejean Fréres workshop. The sample was taken during the renovation and conservation works carried out in the building in 2002 to expand the Fine Arts Thyssen-Bornemisza Museum [1].

2.2. Characterization techniques

The historical glasses with their grisaille paint layers were compositionally and structurally analyzed using FESEM-EDS, LIBS, LIF and the MPEF modality of NLOM.

In-depth cross section imaging was carried out by FESEM with a Hitachi S-4800 cold cathode equipment, working with acceleration voltages of 15 kV. An Oxford X-Max of 20 mm^2 system coupled to the electron microscope with resolution of 125 eV (Mg Kα) was used for EDS microanalyses. The samples were previously coated with carbon as a conductive medium using a JEOL JEE4b sputter. EDS analysis of glasses refers to elemental composition data. However, in glass science and technology, elemental data are mainly formulated in the form of oxides because the elements are commonly bonded between them in the glass lattice by bringing oxygen atoms. Only very few EDS data are expressed as elements, for instance, chlorine that is expressed as chloride (Cl^-). This explains why the quantification of glass components by EDS is done in oxides and not in elements.

LIBS analyses were performed using laser excitation at 266 nm (4th harmonic of a Q-switched Nd:YAG laser, 6 ns pulses, 10 Hz repetition rate) and a 0.30 m spectrograph with a 1200 grooves/mm grating (TMc300 Bentham) coupled to an intensified charged coupled detector (ICCD, 2151 Andor Technologies). The laser beam was conducted to the surface of the base glass and grisaille paint layers by using mirrors at an angle of incidence of 45°. Focusing with a 10 cm focal length lens allowed the achievement of fluences up to 6.6 J cm^{-2} (2 mJ laser pulse energy and 200 μm laser spot diameter). The shot to shot fluctuation of laser energy was less than 10%. LIBS spectra were recorded at 70 nm intervals in the 290–600 nm wavelength range. The spectra were

recorded at a 0.025 nm resolution with a gate delay and width of 100 ns and 3 μs, respectively. For the results presented here, a 300 nm cut-off filter was placed in front of the input window of the spectrograph to reduce scattered laser light from the sample surface and avoid second order diffraction. The spectra resulted from summing up the emissions of the ablation products after ten successive laser pulses, a number that provided good signal-to-noise ratios.

For the LIF measurements we used both the laser source and the spectrograph-ICCD detection system described above for acquisition of LIB spectra. In this case, the time gate was operated with a zero-time delay with respect to the arrival of the laser pulse to the sample surface and with a width of 3 μs. The sample was illuminated through a pinhole, to select the central part of the unfocused laser beam, giving rise to a spot on the sample of elliptical shape with dimensions of 1 mm × 2 mm at an incidence angle of 45° with pulses of around 6×10^{-3} J/cm^2. LIF spectra were recorded at 300 nm intervals in the wavelength range of 275–700 nm using a 300 lines/mm grating. A cut-off filter at 300 nm was also used as for the LIBS measurements. Each spectrum resulted from the accumulation of 25 signal acquired at five different points in each sample zone.

A home made nonlinear optical microscope was used for MPEF measurements. MPEF signals, originated from the focal volume in the sample plane of a mode-locked Ti:Sapphire femtosecond laser, were collected in reflection mode [46,53]. The laser emits at 800 nm, with an average power of 680 mW, delivering 70 fs pulses at a repetition rate of 80 MHz. Before performing the present NLOM measurements, we determined the laser parameters that ensure safe measurement conditions using the procedure described in previous works [46,47,53], that relies in the online monitoring and visualization by a CCD camera of possible changes in the surface or inner layers of the substrate due to femtosecond laser excitation upon repetitive irradiation. A variable neutral density filter (NDC-50C-2M, Thorlabs) served to control the laser power reaching the sample. For the current measurements, the average power was in the range of 6–9 mW. The laser beam was modulated using a chopper at a frequency of 130 Hz and conducted to the sample through the aperture of a microscope objective lens (M Plan Apo HL 50X, Mitutoyo, NA 0.42) by using a dichroic beam splitter (FF750-SDi02-25x36, Semrock) with a high reflection at 800 nm. The focal plane of the laser was selected with motorized translation XYZ stages (Standa 8MVT100-25-1 for XY and Standa 8MTF for Z). The lateral and axial resolutions achieved are of 1 and 2 μm, respectively. In what regards the lateral resolution, it was determined by imaging the focus of the laser spot on the surface of the sample with a CCD camera that also served for online monitoring the MPEF signal acquisition. In turn, the axial resolution was tested by measuring the thickness of commercial standard PET thin films by MPEF (nominal thicknesses of 10, 20, 30, 50 and 75 μm). The intensity of MPEF signals during Z-scans with steps of 1 μm varied appreciably every two steps (2 μm). The measured thicknesses on PET films were found in good agreement with those specified by the provider. A LabVIEW interface controlled both scanning and data acquisition procedures. MPEF signals were collected in the backward direction through the microscope objective lens and a beam splitter (70/30) and measured using a photomultiplier tube (9783B, ET Enterprises) connected to a lock-in amplifier (SR810 DSP, Stanford Research Systems) to ensure high amplification and signal-to-noise ratio. To cut off the reflected excitation laser light, a short pass filter (335–610 nm, Thorlabs FGB37S) was placed at the entrance of the photomultiplier. The remaining 30% of the MPEF signal was sent to a CCD camera (Thorlabs DCC1645C) for online visualization of the sample surface. The photon dose applied to the surface of the sample was 80×10^6 pulses/point. Each MPEF profile resulted from 300 measurements during the whole Z-scan using a step of 1 μm/per second, then the time required to complete each MPEF profile corresponds to 5 min. The thickness value of each grisaille paint was obtained by averaging the values obtained in Z-scans carried out in five different points of each sample.

3. Results and discussion

3.1. Field emission scanning electron microscopy/energy-dispersive X-Ray spectroscopy

FESEM-EDS cross-section micrographs and chemical microanalyses were carried out both on the glass body or on the grisaille paints and were used to assess the chemical composition and features of the grisailles paint layers, including their thickness in different areas, the degree of adherence to the base glass, their homogeneity and their state of conservation. Results are displayed in Fig. 2 and Table 2 which differentiates the wt % of components in areas of the glass body and of the grisaille paint layer (squares marked as 1 and 2 respectively in the figure).

The FESEM cross-section micrograph of the Balmaseda sample is shown in Fig. 2A. The EDS microanalyses of the glass body indicate the presence of sodium, aluminum, silicon and calcium oxides. The presence of 12.4 wt % of sodium oxide is indicative of a soda lime silicate glass. The grisaille paint layer appears poorly densified showing fragments with spiky edges, and without good adherence to the base glass. This grisaille has not undergone a softening/melting process indicating that is not the original but is part of a recent restoration. The EDS microanalysis indicates that it is mainly composed of silicon, aluminum, lead, zinc, iron, chromium and cobalt oxides. Among these components, iron, chromium and cobalt oxides could be the chromophores and are responsible of its black-brown coloration. The flux used for the grisaille elaboration is mainly composed by lead, silicon and zinc oxides which are the main components of traditional grisailles. The observed microstructure with the aspect of the interface in between the base glass and the grisaille indicates that during the grisaille manufacturing the softening/melting temperature was not reached. This issue indicates that the Balmaseda grisaille is not original but the result of a restoration process. The restoration criteria advice to avoid heat treatments of either the grisailles or the base glasses; reversible cold enamel based on water should be used for repainting the damaged grisaille. Such strategy is more adequate than the use of a traditional grisaille without heat-treatment, which would be poorly adhered onto the base glass, as shown by FESEM.

Fig. 2B displays the FESEM cross-section micrograph of the Girona sample. Table 2 shows the results of the EDS microanalyses carried out on different areas of the body glass (analysis 1) and the grisaille (analysis 2). The results of the EDS microanalysis carried out on the body glass indicate that it is a potash lime silicate glass, with 22.9 wt % of potassium oxide. The grisaille of Girona sample (Fig. 2B) shows both good appearance and homogeneity, and it is well adhered to the base glass. It is composed of sulfur, antimony and mercury oxides as main components, and aluminum and potassium oxides as minor components. Antimony is the pigment responsible for the grisaille color, and with mercury they are the components used as flux for the glass melting.

Fig. 2C shows the FESEM cross-section micrograph of the León sample. Table 2 summarizes the EDS results in areas of the body glass (analysis 1) and the corresponding to the grisaille paint layer (analysis 2). The results of the EDS microanalysis carried out on the body glass indicate that it is a potash lime silicate glass, with 16.8 wt % of potassium oxide. The FESEM micrograph shows a well-densified grisaille although its thickness is not homogeneous, which could be due to some sort of degradation process that has undergone over the years. Its composition is based on silicon, iron and lead oxides, and calcium, aluminum and potassium oxides as minor components. Iron oxides are responsible for the grisaille color, while lead and silicon oxides act as a flux.

Finaly, Fig. 2D displays FESEM cross-section micrograph of the Goyeneche sample, and the corresponding EDS results are displayed in Table 2 for areas of the body glass (analysis 1) and the grisaille paint layer (analysis 2). The results of the EDS microanalyses carried out on the body glass indicate that it is a soda lime silicate glass, with 12.0 wt %

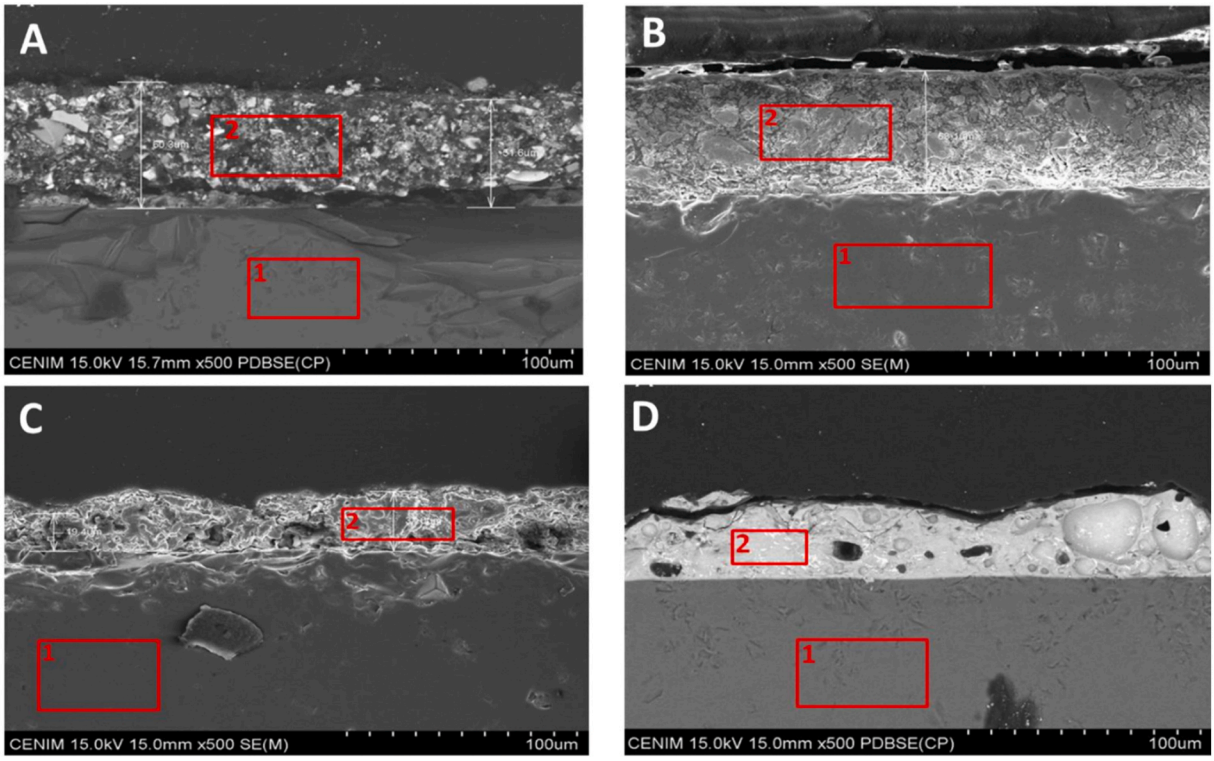

Fig. 2. FESEM micrographs of grisaille paint layers on glasses from the different samples of stained-glass windows: A) Balmaseda, B) Girona, C) León and D) Goyeneche. Squares labelled 1 and 2 refer to areas of the glass body and of the grisaille paint layer, respectively.

Table 2
Results (wt %) of EDS microanalyses carried out on different areas of the cross-sections of samples.

Samples	Balmaseda		Girona		León		Goyeneche	
	Glass body	Grisaille	Glass body	Grisaille	Glass body	Grisaille	Glass body	Grisaille
Na_2O	12.4	–	1.3	–	3.7	–	12.0	7.4
Al_2O_3	0.6	1.6	1.4	0.6	0.8	2.1	0.7	0.8
SiO_2	73.0	26.7	69.4	–	54.0	25.7	73.7	27.9
SO_3	–	–	–	39.7	–	–	–	–
Cl^-	–	–	0.3	–	0.6	–	0.2	–
K_2O	–	–	22.9	0.7	16.8	1.4	1.6	1.7
CaO	14.0	–	4.7	–	9.8	3.3	10.4	0.9
MgO	–	–	–	–	7.5	–	–	–
Cr_2O_3	–	8.1	–	–	–	–	–	–
Fe_2O_3	–	18.5	–	–	1.0	33.6	0.5	30.0
Sb_2O_3	–	–	–	38.0	–	–	–	–
P_2O_5	–	–	–	–	5.0	–	–	–
CoO	–	5.5	–	–	–	–	–	–
ZnO	–	9.0	–	–	–	–	–	–
MnO	–	–	–	–	0.8	–	0.9	3.0
CuO	–	–	–	–	–	–	–	6.0
PbO	–	30.6	–	–	–	33.9	–	22.3
HgO	–	–	–	21.0	–	–	–	–

of sodium oxide. The grisaille paint layer appears well-densified and adhered to the base glass, even though it presents much inner heterogeneities such as large bubbles and irregular surface. Its composition is mainly formed by silicon, sodium, lead, iron and copper oxides. As minor components, calcium, aluminum, potassium and manganese oxides are detected. The color of the grisaille is due to the mixture of various pigments based on iron, manganese and copper oxides, with lead oxide and silicon dioxide as a glass flux.

Glass and grisaille compositions identified for these samples are commonly found throughout the historical development of stained-glass windows. Potash lime silicate glasses are well documented in Medieval stained glass examples [2,52] and also in evolved potash lime silicate glasses with a higher chemical stability from the seventeenth and eighteenth centuries [7,51]. Soda lime silicate glasses are well-known in stained glass windows from the nineteenth and twentieth centuries [1,6,7,12]. In addition, components found in grisailles, mainly lead and iron oxides in the ancient ones from the Cathedral of León (thirteenth-fourteenth centuries) [2,5,52], and a more extensive range of oxides such as antimony, zinc, chromium, manganese, copper, etc., as in the samples of Balmaseda and Goyeneche from the nineteenth and twentieth centuries, are also well documented in stained glass windows of similar chronologies [1,6,7,12].

The thicknesses of the grisaille paint layers were retrieved from FESEM cross-section images. The images reveal the inhomogeneous thickness of each grisaille paint layer and highlight the presence of bubbles and micrometric particulates, as expected in the hand-made

craft process involved in the decoration of the stained-glass window. The mean thickness values and standard deviation obtained through measurements undertaken on 5 different areas for each sample show values of 50 ± 9, 78 ± 30, 26 ± 6 and 36 ± 12 μm for grisaille paint layers from Balmaseda, Girona, León and Goyeneche sites, respectively.

3.2. Laser induced breakdown spectroscopy

LIB spectra displayed in Fig. 3 were recorded on the body glass samples (left columns) and on their corresponding grisaille paint layers (right columns). The assignement of the spectral lines was done based on data from the NIST database [54].

Fig. 3 A shows the LIB spectrum on the body glass for the Balmaseda sample. The spectrum reveals its elemental composition by virtue of the emission lines of the major and minor components. These are iron (Fe), silicon (Si), calcium (Ca), aluminum (Al), titanium (Ti), potasium (K), lead (Pb), strontium (Sr), barium (Ba), sodium (Na) and calcium (Ca) oxides. The elements Si, Ca, Al, K and Na correspond to the main glass components. The other minor components (Ti, Pb, Ba and Sr) can be attributed to impurities of the raw materials employed in the manufacturing process and to stabilizing agents.

In the other three examined body glasses, Girona, León and Goyeneche samples (Fig. 3C, E, G), in addition to the elements observed for Balmaseda body glass sample, lines of manganese (Mn), copper (Cu), cobalt (Co) and magnesium (Mg) were detected. These elements, in addition with Fe, are linked to the presence of chromophores which are responsible of the glass coloration. Balmaseda and Goyeneche glass samples show a high content of Na and a lower contribution of K; however, for Girona and León glasses the content of K increases and the corresponding to Na decreases. This fact could indicate that the Balmaseda and Goyeneche glasses are mostly soda lime silicate glasses, and the Girona and León glasses are potash lime silicate glasses. These suggestions were corroborated by EDS results (Table 2).

LIB spectra acquired on the four studied grisailles are richer in line emissions than those corresponding to their base glass substrates due to a high variety of metal oxides and maybe impurities dispersed in the glassy matrix or flux oxides (SiO_2, PbO). Fig. 3B shows the LIB spectrum of grisaille from the Balmaseda sample revealing the presence of line emissions of Fe, Si, Ca, Al, Cu, Ti, Co, Mn, K, Pb, Cr, Zn, Sr, Ba, Na and CaO. Si and Pb lines confirm the presence of silicon and lead oxides as the base of glassy matrix for this grisaille, compounds that are responsible for the grisaille adherence to the glass substrate after firing. PbO is used to get lower melting temperatures and thus avoiding thermal bending or other deformation in the glass substrate. The oxide compounds based on Fe, Cu, Co, Mn and Cr are used as agents responsible for the grisaille coloration. The observed brown coloration can be mainly attributed to its high content of iron oxide. The rest of the components (Ca, Al, Ti, K, Zn, Sr, Ba and Na) could be considered as impurities, stabilizer agents and elements used in the manufacturing of the base glass.

Fig. 3F, H show LIB spectra derived from the grisailles of the León and Goyeneche samples revealing a qualitatively similar compostions except for the presence of chromiun in the latter. The black hue of these two grisailles is due to the presence of coloring agents almost similar to those observed for the Balmaseda grisaille which contains low content of iron oxide. However, the grisaille on the stained-glass from the Girona

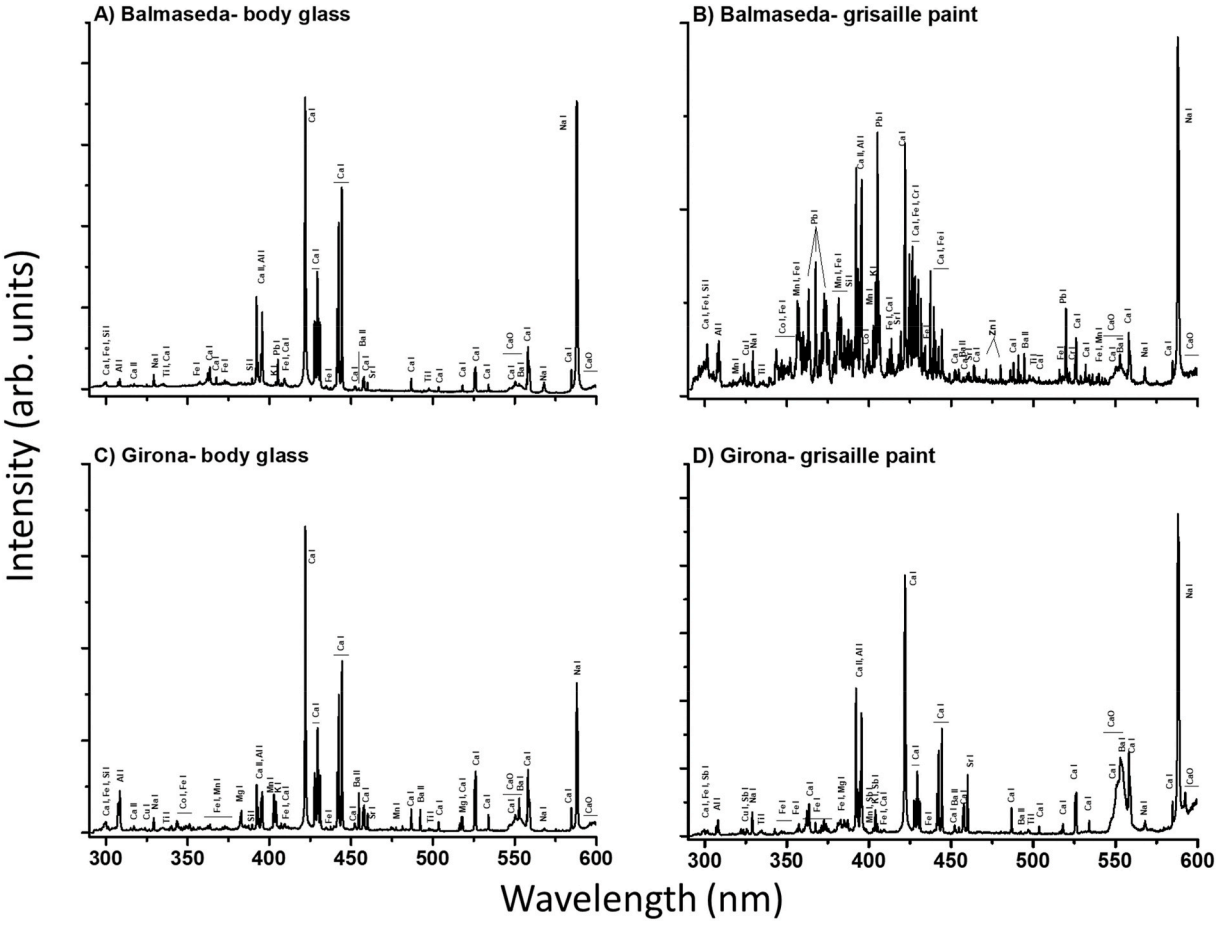

Fig. 3. Representative LIB spectra of historical body glass samples (left columns) with their corresponding grisaille paint layer (right columns). The LIB spectra correspond to the accumulation of 10 laser pulses. The time delay and gate width were 100 ns and 3 μs, respectively. The symbols I and II indicate the neutral and singly ionized species, respectively.

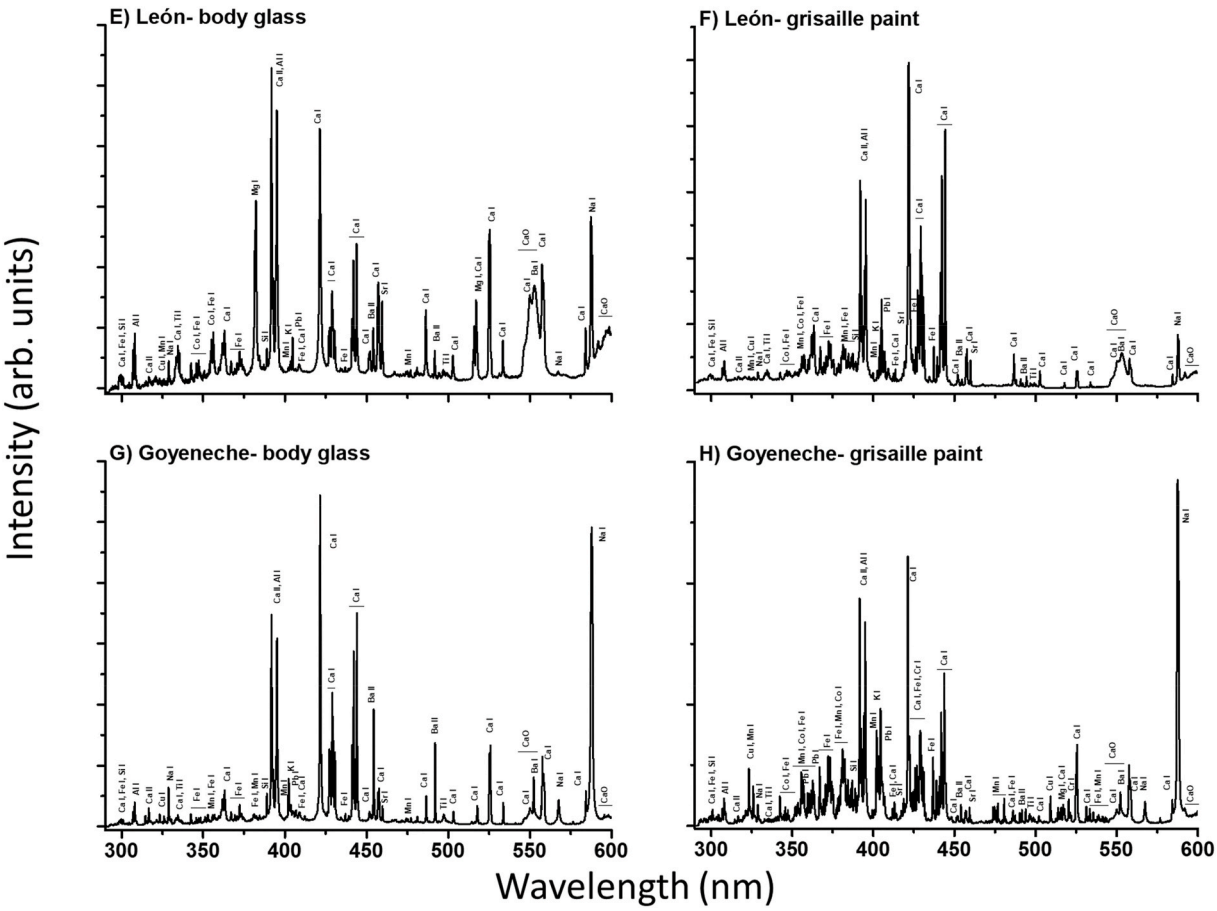

Fig. 3. (*continued*).

sample (Fig. 3D) shows a different composition than the previous ones: mainly the use of antimony oxide as a glassy matrix instead of lead and silicon oxides which also acts as a fining agent for removing bubbles. In this case the number of colorant agents used is lower and consist of Cu, Mn and Fe.

Table 3 presents a summary of the elemental composition of each historical glass sample with its corresponding grisaille as determined by LIBS. The comparison with data derived from EDS (Table 2) reveals that LIBS is able to detect the presence of most of the elements in the compounds identified by EDS, except the elements P, S, Cl, Hg and As. This is due to the difficulty to detect these elements in the considered spectral range (290–600 nm), inhomogeneities in the grisaille composition and/or to their very low content. However, it was observed that a high number of other elements were detected by LIBS which were not posible to be detected by EDS.

The obtained LIBS results are indicative of the high sensitivity of the LIBS technique when applied to the characterization of grisailles that in some cases is superior to that achieved by other more established analytical techniques used for elemental analysis of historical glass. As shown, LIBS could provide several advantages even for qualitative analysis, as this technique can easily determine the presence of light and trace elements and chromophores, which yield valuable information on the chronology and manufacturing of the historical stained glasses. In our case, the use of LIBS has allowed us to determine the chemical nature of the matrix of the glasses and their corresponding grisailles and to highlight the possible differences in their composition.

Table 3
Elemental composition of the body glass and its corresponding grisaille paint layer samples obtained through LIBS measurements. The main elemental components are indicated in bold.

Samples		Elemental composition
Balmaseda	Body glass	Fe, Si, **Ca**, Al, Ti, K, **Pb**, Sr, Ba, **Na**, CaO.
	Grisaille	**Fe**, Si, Ca, Al, **Cu**, Ti, **Co**, **Mn**, **K**, **Pb**, **Cr**, **Zn**, Sr, Ba, **Na**, CaO.
Girona	Body glass	Fe, Si, **Ca**, Al, Cu, Ti, **Co**, **Mg**, **Mn**, **K**, Sr, **Ba**, Na, CaO.
	Grisaille	**Fe**, Ca, Al, **Cu**, **Sb**, Ti, Mg, Mn, K, Sr, Ba, **Na**, CaO.
León	Body glass	**Fe**, Si, **Ca**, Al, **Cu**, Ti, **Co**, **Mg**, **Mn**, **K**, Pb, Sr, **Ba**, Na, CaO.
	Grisaille	**Fe**, Si, Ca, Al, Cu, Ti, Co, **Mn**, **K**, **Pb**, Sr, Ba, Na, CaO.
Goyeneche	Body glass	Fe, Si, **Ca,** Al, **Cu**, Ti, **Mn**, K, **Pb**, Sr, **Ba**, **Na**, CaO.
	Grisaille	**Fe**, Si, Ca, Al, **Cu**, Ti, **Co**, **Mn**, K, **Pb**, **Cr**, Sr, Ba, Na, CaO.

3.3. Laser Induced Fluorescence

Representative LIF spectra collected on the body surface of the glasses and on the corresponding grisailles for each of the four historic stained glasses are shown in Fig. 4. In addition, Fig. 4A displays a multi-Gaussian fit of the LIF spectra from Balmaseda sample indicating the presence of an additional band around 325 nm for grisaille paint layer compared to the glass body.

All collected spectra display two broad bands centered at 360 and 440 nm, although the relative intensities and spectral profiles vary from one sample to another. For the body glasses (black lines), these bands are mainly assigned to oxygen deficiency centers [39,41] although the band at 360 nm may have also contributions from Fe^{2+}/Fe^{3+} chromophores [25]. The presence of different contents of metallic chromophores such as cobalt, copper, manganese and iron (Table 2) account for the diverse

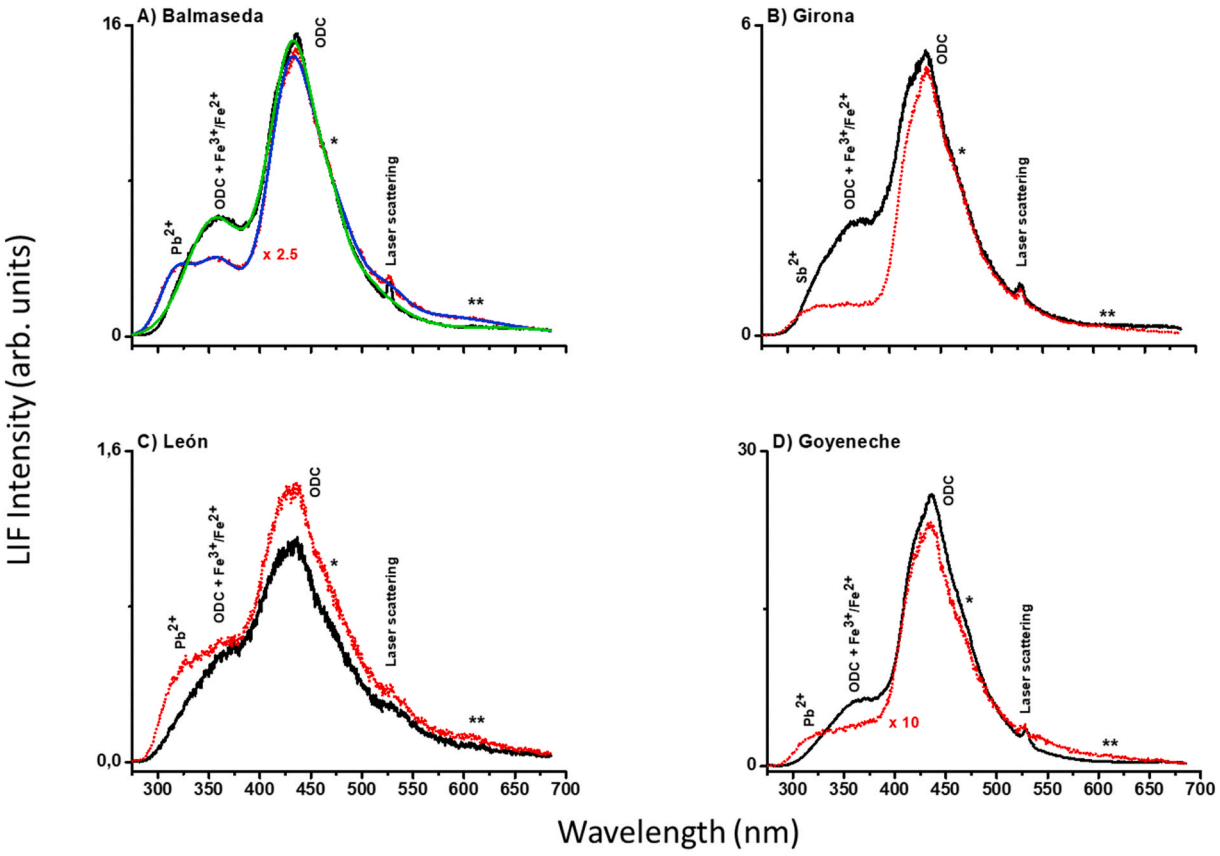

Fig. 4. LIF spectra of body glass (in black) and the corresponding grisaille paint layers (in red). Fig. 4A, shows a multi-Gaussian fits in green and blue colors for fluorescence emissions from glass body and grisaille paint layer, respectively. The feature at 532 nm corresponds to laser light scattering. The single and double asterisks mark the position of bands assigned to Cu^{2+} and Mn^{3+} oxides, respectively. ODC indicates oxygen deficiency centers. The time delay and gate width were set to zero and 3 μs, respectively. Spectral resolution was 5 nm. (For interpretation of the references to color in this figure legend, the reader is referred to the Web version of this article.)

coloration of the body glasses, colourless for Balmaseda, blue for Girona, green-bluish for León and green-yellowish for Goyeneche samples. The contribution of these chromophores to the fluorescence emission is not much evident due to the expected reabsorption of the fluorescence emitted by the chromophores, all presenting absorption bands in the near-UV and Visible spectral ranges [55]. Despite this, the shoulder at 475 nm and the weak band at 610 nm have been tentatively assigned to Cu^{2+} and Mn^{3+} ions [25].

For the Balmaseda sample (Fig. 4A), the overall decrease in the fluorescence intensity of the grisaille paint layer (red line) with respect to that of body glass (black line) by a factor of 3 is accompanied, as commented before, with the appearance of a new additional band around 325 nm which corresponds to Pb^{2+}/Sn^{2+} chromophores [40,56,57] from PbO_2/SnO_2, main components of grisaille paint layers with SiO_2. EDS and LIBS results reported above corroborate these differences. In addition, the LIF spectra of this sample show also the weak shoulders centered at around 475 and 610 nm, which are overimposed on the tail of the main fluorescence band at 440 nm; and ascribed to the presence of Cu^{2+} and Mn^{3+} chromophores [25,57].

The remaining analyzed body glasses and grisailles (in Fig. 4B–D) show similar LIF emission features than those obtained for the Balmaseda sample. The low LIF intensity observed for Girona and León body glasses (3 and 10 times respectively less intense than the signal corresponding to the Balmaseda sample) is due to their low content of SiO_2, main component of glasses, as revealed by EDS results. Goyeneche glass body shows the highest emission fluorescence intensity.

In terms of comparison, the integrated fluorescence emission from the Balmaseda grisaille layer was found around 1.5 times higher than that from Girona one and 3 times higher than those from León and Goyeneche samples.

3.4. *Multiphoton excitation fluorescence*

Due to the behaviour of the fluorescence emission of the body glasses and grisaille paint layers examined by LIF (Section 3.3.), the femtosecond laser at 800 nm is expected to generate two- and/or three-photon excitation fluorescence in the range selected for the collection of signals (335–610 nm). Asignment of the fluorescence bands allow to conclude that these emissions are due both to the flux components ($PbO–SiO_2$/Sb_2O_3) and to the different metallic oxides of grisailles, with different contributions for each sample [6–8]. Furthermore, the absorption/reflectance of laser light at 800 nm measured for the grisaille paint layers (around 95% in all samples) suggests that some scattering of the incident laser light and/or partial attenuation of the generated nonlinear signal should be taken into account during the analysis of the MPEF signals.

An in-depth scan of the grisaille paint layers was performed by MPEF in different areas to compensate for the heterogeneities due to the presence of bubbles and micrometric particles and to irregularities in their surface topography and thickness, as revealed by FESEM results shown in section 3.1. MPEF signal intensities were measured as a function of depth from the surface of the samples in steps of 1 μm/s. Representative profiles for each grisaille sample are shown in Fig. 5. Although an empirical approach, not based on optical propagation principles could be misleading, fitting of the obtained MPEF profiles was attempted by using Gaussian, Voight and Lorentzian functions. The best fit, and better agreement of thickness values with those retrieved by FESEM, was obtained using a Lorentzian function allowing the determination of the apparent grisaille paint layer thickness by means of the

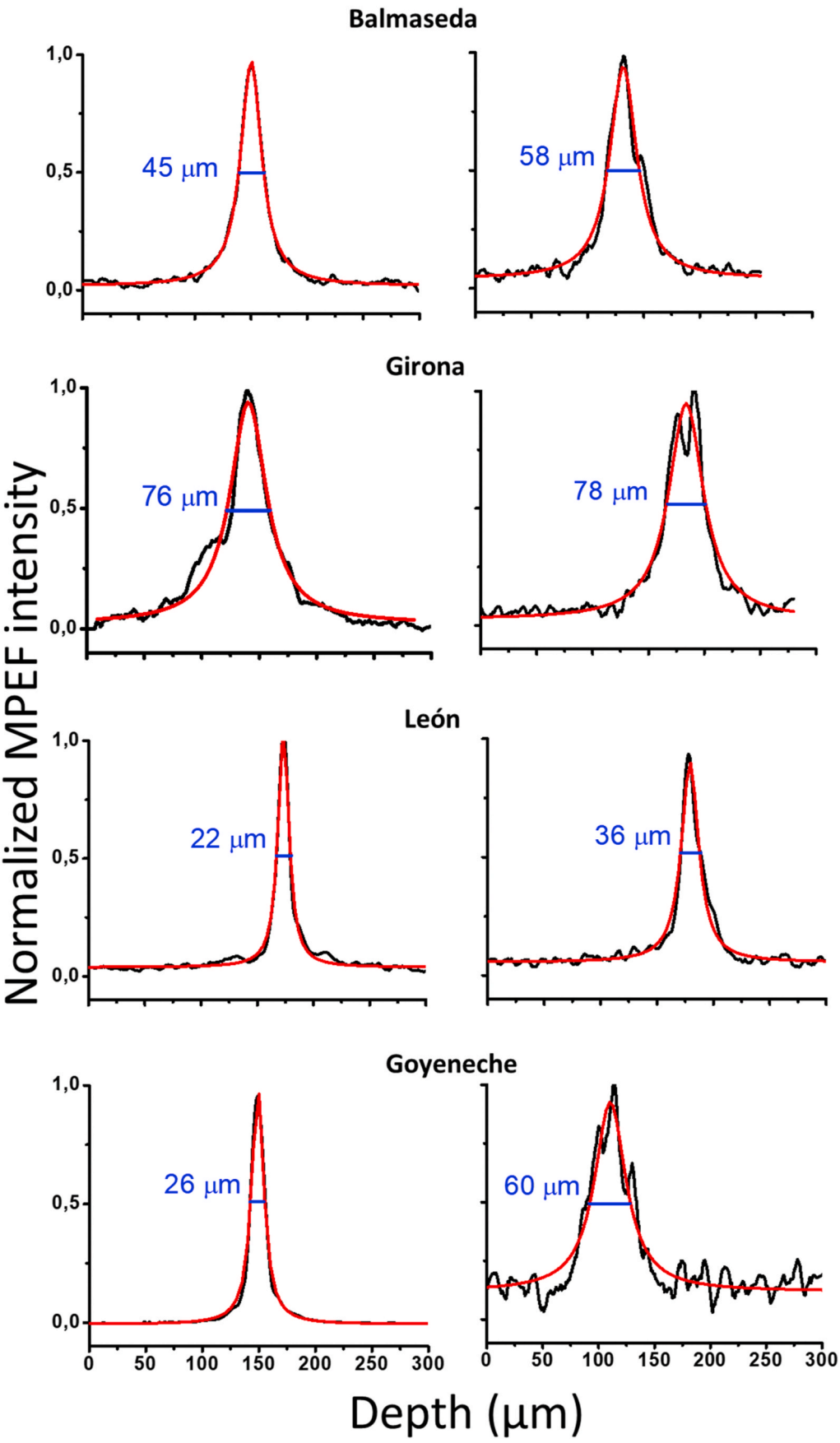

Fig. 5. Depth scans of the MPEF signals (in black) upon analysis of historical glass grisailles and fits by Lorentzian functions (in red). The thicknesses of the grisaille paints (in blue) are given by the FWHM values of the fits after refractive index corrections. Profiles from different zones, showing the lowest and highest thickness values for the same grisaille paint layer are presented in the left and right columns, respectively. (For interpretation of the references to color in this figure legend, the reader is referred to the Web version of this article.)

full width at half maximum (FWHM). Although the MPEF intensities of the four grisaille layers are presented normalized in Fig. 5, the most intense emission was detected in grisailles of Balmaseda and Girona samples, whereas weaker non-linear signals were collected from León and Goyeneche samples, in accordance with the fluorescence behaviour obtained during LIF analysis.

The real thickness of the grisaille paint layers was calculated by correcting the obtained FWHM values with the apparent depth correction factor ($\mathbf{F} = \frac{1-\sqrt{1-\mathbf{NA}^2}}{\mathbf{n}-\sqrt{\mathbf{n}^2-\mathbf{NA}^2}}$) [53,58], which considers the effective numerical aperture NA of the focusing objective lens (0.42) and the refractive index n of the analyzed material. The grisaille paint layers are mainly made up of metallic oxides (Fe, Pb, Sb, Si, etc.) and we have calculated an average value of $n \approx 1.92$ based on the refractive indexes tabulated in Ref. [59]. The correction factor depends on the material refractive index and its estimation could directly affect the thickness estimation values. However, we believe that the calculated average value of n for the different considered grisaille paint layers, around 1.92, could only slightly deviate from this value, and would not affect considerably the calculated correction factor, with a value of around 2, and therefore the thickness determination. This assumption was confirmed by the good agreement between the obtained FESEM and MPEF results. The average thickness values with their standard deviation obtained by MPEF for the different grisalle paint layers are shown in Table 4.

The MPEF results showed good agreement with the cross-section measurements obtained by FESEM for all the four grisaille paint layers considered, as listed in Table 4. The measurements presented herein were carried out under safe conditions. First, the average laser power used to measure the MPEF signals is far from the damage threshold of the grisaille paint layers (as monitored through CCD online visualization of the sample surface during femtosecond laser excitation). Optical scattering, reabsorption of the emitted fluorescence and single-photon absorption of the 800 mm excitation beam by some of the grisaille paint components could influence the thickness determination by affecting the intensity of the MPEF. Notwithstanding these effects, a sufficient in-depth penetration of the femtosecond laser radiation and enough degree of transparency in the spectral range where the MPEF signal is detected, produces sufficiently high MPEF signals for all grisaille paint layers studied, allowing to retrieve the thickness of the gisaille values as shown.

SHG and THG NLOM modalities, could also be used for studying grisaille paint layers. SHG is expected to be generated by the presence of media based on crystalline or highly organized structures without inversion symmetry. If grisaille layers contain some crystalline material, the SHG signal upon excitation at 800 nm could be discriminated from the emitted multi-photon fluorescence with the help of a narrowband filter centered at 400 nm. In turn, THG would help to determine the position of the layer boundaries, but in the case of the studied samples, a retroreflection configuration is needed implying the use of a microscope objective with high transmission in the UV region. Although work is in progress with the samples of this study to perform measurements using these NLOM modalities, the results shown herein demonstrate that the proper choice of laser excitation wavelength, average power and spectral range for collection of the fluorescence signal is of high importance to ensure a correct estimation of grisaille paint layer thickness by MPEF in a non-invasive approach.

Table 4
Comparison between the mean thickness value and standard deviation (in μm) of grisaille paint layers determined by MPEF (measurements from 5 positions along the grisaille width) and FESEM on samples from historical stained glasses.

Grisaille paint layers	MPEF	FESEM
Balmaseda	51 ± 7	50 ± 9
Girona	77 ± 1	78 ± 30
León	29 ± 7	26 ± 6
Goyeneche	43 ± 17	36 ± 12

Given the results obtained, it is worth highlighting the advantages of NLOM for cultural heritage applications compared to confocal microscopy based on single photon excitation fluorescence configuration. In conventional confocal laser scanning microscopy, the excitation source for fluorescence is usually a highly focused visible and ultraviolet wavelength CW laser beam. The waist of the laser beam is recreated in a hole (the confocal aperture), which prevents fluorescence generated outside the focal plane from reaching the detector. Fluorescence intensity measurement allows a point-by-point 3D image to be constructed while sequentially scanning the laser spot or sample stage in all three dimensions.

Confocal microscopes, currently used in different research laboratories, do have limitations. The out of focus excitation, which does not contribute to the 3D image, increases the potential of damage to the analyzed material, and the visible and ultraviolet wavelengths, optimal for direct excitation and highly absorbed, do not penetrate deeply into materials. Furthermore, re-imaging the fluorescence from the focus of the laser beam onto the confocal aperture generates losses and reduces sensitivity. These factors limit the ability to image deeply into the samples or objects under study. The use of femtosecond lasers for MPEF overcomes these limitations. The high peak power of femtosecond pulses (typically at a repetition rate of 80 MHz), together with the high numerical aperture microscope objective, generate enough photon densities within the focal volume to drive two- and even three-photon absorption. Elsewhere in the sample, the power density is too low for nonlinear excitation, so there is an inherent spatial sectioning capability that obviates the need for a confocal pinhole. This means that the detector can be located close to the material, resulting in increased sensitivity and signal-to-noise ratio. There is also virtually no out-of-focus excitation inducing significantly less or no photobleaching and material damage. Moreover, because NLOM uses longer wavelengths in the IR, where there is less absorption and scattering, the MPEF technique can penetrate much farther into the sample (hundreds *vs* tens of micrometers). In addition to the multiphoton generated fluorescence, SHG and THG of the fundamental IR frequency of the excitation femtosecond laser do not require fluorescent chromophores but, as indicated above, spatially ordered structures of molecules with certain symmetry for SHG or differences in refractive index and third-order susceptibility and dispersion for THG. Thus, in a single set-up, these two modalities of NLOM, also benefitting from the high peak power of the femtosecond source, non-invasively provide complementary 3D information on the structure and composition of the sample.

The work presented in this manuscript makes use of a laboratory-based nonlinear optical microscope that, due to the size of the femtosecond laser source and of the microscope setup, is not suitable for in-situ measurements in historical glass windows. However, our NLOM system allows high operation flexibility, due to the use of stable and robust 3D translation stage and a long working distance objective, and has the capacity to analyse samples of medium size as large as 40× 50 cm^2, the size limitation being related with the scanning capacity of the system. One of the main goals of the work shown has been to assess the capacity of NLOM for non-destructive analysis of historical glass objects and to compare results with those obtained by other more conventional techniques. Therefore, the use in this work of a laboratory-based system is duly justified. Notwithstanding, it is important to say that, due to the rapid advances in femtosecond laser technology and optical component arrangements, it will not take long to dispose of portable systems to carry out NLOM measurements on cultural heritage objects in a museum or in heritage building environments [60].

4. Conclusions

The capabilities of non-invasive determination of the thickness of different grisaille paint layers from historic stained-glass windows have

been explored using MPEF microscopy. Complementary characterization of the composition of grisaille materials was obtained through a multi-analytical approach, where the spectral information provided by LIF measurements allowed determination of the NLOM measurement conditions and supported the interpretation of the results. LIBS and EDS allowed the determination of elemental composition of the body glasses and their corresponding grisaille paint layers. Finally, FESEM served to quantify the grisaille thicknesses in a destructive way for comparison with the values obtained using non-destructive MPEF.

Fluorescence emissions obtained upon laser excitation at 266 nm provided further information about the nature of the body glasses and their corresponding grisaille paint layers, indicating the presence of chromophores responsible of the coloration and the main oxide components which take part in the composition of the studied substrates. Analysis by LIBS of the glass samples of this study allowed the detection of major, minor and trace elements in body glasses and grisailles with higher sensitivity for major and minor components than EDS, confirming LIBS as a powerful technique to determine the elemental composition and to look for chemical differences or similarities in composition of non-destructible samples with historical and heritage value. The speed of analysis achieved with this technique facilitates the examination of a large number of samples in the field, at excavation sites, in museums, cathedrals and other civil buildings.

The results obtained using the above techniques served to select the adequate excitation and signal collection conditions for studying the grisaille paint layers on historical stained-glass windows by the cutting-edge MPEF technique, a modality of NLOM never applied before on grisaille paint layers. Upon femtosecond laser excitation at 800 nm, and applying average powers far below the grisaille paints damage thresholds, it was possible to determine the grisaille paint layer thickness through this technique. The good agreement between the thickness values estimated with MPEF and FESEM serves to validate the former technique for grisaille paint layers that display sufficient degree of transparency to the excitation laser wavelength and in the spectral range of the emitted fluorescence. The MPEF measurements described here were carried out in the reflection mode, thus providing the possibility to apply this methodology to measure coatings of grisaille materials laying on a glass substrate in non-destructive way. Further research is in progress on grisaille paint layers by combining MPFE with other modalities of NLOM such as Second and Third Harmonic Generation.

Declaration of competing interest

The authors declare that they have no known competing financial interests or personal relationships that could have appeared to influence the work reported in this paper.

Acknowledgments

This research has been funded by the Spanish State Research Agency (AEI) through projects PID2019-104124RB-I00/AEI/10.13039/501100011033 and PID2019-104220RB-I00/AEI/10.13039/501100011033, by project TOP Heritage-CM (S2018/NMT-4372) from Community of Madrid, by the H2020 European project IPERION HS (Integrated Platform for the European Research Infrastructure ON Heritage Science, GA 871034) and supported by CSIC Interdisciplinary Platform “Open Heritage: Research and Society” (PTI-PAIS). M.O. thanks CSIC for a contract. Finally, the authors acknowledge professional support from the TechnoHeritage Network of Science and Technology for the Conservation of Cultural Heritage.

Appendix A. Supplementary data

Supplementary data to this article can be found online at https://doi.org/10.1016/j.talanta.2021.122314.

Statement contribution of authors

Dear editor

Below is the contribution of each author to the manuscript entitled “Multiphoton Excitation Fluorescence Microscopy and Spectroscopic Multianalytical Approach for Characterization of Historical Glass Grisailles” by M. Oujja, F. Agua, M. Sanz, D. Morales-Martin, M. García-Heras, M.A. Villegas and M. Castillejo submitted for consideration to Talanta. M. Oujja and F. Agua: Methodology, Investigation, Formal analysis, Writing - Review & Editing. M. Sanz, D. Morales-Martin and M. García-Heras: Methodology, Investigation, Formal analysis, Review & Editing. M.A. Villegas and M. Castillejo: Supervision, Funding acquisition, Project administration, Review & Editing.

References

[1] M. García-Heras, N. Carmona, C. Gil, M.A. Villegas, Neorenaissance/Neobaroque stained glass windows from Madrid: a characterisation study on some panels signed by the Maumejean Fréres company, J. Cult. Herit. 6 (2005) 91–98, https://doi.org/10.1016/j.culher.2004.12.001.

[2] N. Carmona, M.A. Villegas, J.M.F. Navarro, Study of glasses with grisailles from historic stained glass windows of the cathedral of León (Spain), Appl. Surf. Sci. 252 (2006) 5936–5945, https://doi.org/10.1016/j.apsusc.2005.08.023.

[3] T. Rehren, I.C. Freestone, Ancient glass: from kaleidoscope to crystal ball, J. Archaeol. Sci. 56 (2015) 233–241, https://doi.org/10.1016/j.jas.2015.02.021.

[4] W. Meulebroeck, H. Wouters, K. Nys, H. Thienpont, Authenticity screening of stained glass windows using optical spectroscopy, Sci. Rep. 6 (2016) 37726, https://doi.org/10.1038/srep37726.

[5] N. Capobianco, M.O.J.Y. Hunault, S. Balcon-Berry, L. Galoisy, D. Sandron, G. Calas, The Grande Rose of the Reims Cathedral: an eight-century perspective on the colour management of medieval stained glass, Sci. Rep. 9 (2019) 3287, https://doi.org/10.1038/s41598-019-39740-y.

[6] O. Schalm, Characterization of Paint Layers in Stained-Glass Windows: Main Causes of the Degradation of Nineteenth Century Grisaille Paint Layers, Universiteit Antwerpen, 2000.

[7] T. Pradell, G. Molina, S. Murcia, R. Ibáñez, C. Liu, J. Molera, A.J. Shortland, Materials, techniques, and conservation of historic stained glass “grisailles”, Int. J. Appl. Glass Sci. 7 (2016) 41–58, https://doi.org/10.1111/ijag.12125.

[8] C. Machado, A. Machado, T. Palomar, M. Vilarigues, Grisaille in historical written sources, J. Glass Stud. 61 (2019) 71–86, https://doi.org/10.2307/26862829.

[9] M. García-Heras, C. Gil, N. Carmona, M.A. Villegas, Weathering effects on materials from historical stained glass windows, Mater. Construcción 53 (2003) 21–34, https://doi.org/10.3989/mc.2003.v53.i270.271.

[10] N. Carmona, M.A. Villegas, J.M.F. Navarro, Characterisation of an intermediate decay phenomenon of historical glasses, J. Mater. Sci. 41 (2006) 2339–2346, https://doi.org/10.1007/s10853-005-3948-6.

[11] M. García-Heras, N. Carmona, A. Ruiz-Conde, P. Sánchez-Soto, J.J. Benítez, Application of atomic force microscopy to the study of glass decay, Mater. Char. 55 (2005) 272–280, https://doi.org/10.1016/j.matchar.2005.07.001.

[12] O. Schalm, K. Janssens, J. Caen, Characterization of the main causes of deterioration of grisaille paint layers in 19th century stained-glass windows by J.-B. Capronnier, in: Spectrochim. Acta - Part B At. Spectrosc., Elsevier, 2003, pp. 589–607, https://doi.org/10.1016/S0584-8547(02)00282-3.

[13] A. Atrei, A. Scala, M. Giamello, M. Uva, R.M. Pulselli, N. Marchettini, Chemical composition and micro morphology of golden laminae in the wall painting “La maestà” by simone martini: a study by optical microscopy, XRD, FESEM-EDS and ToF-SIMS, Appl. Sci. 9 (2019) 3452, https://doi.org/10.3390/app9173452.

[14] M. Rahrig, M. Torge, 3D inspection of the restoration and conservation of stained glass windows using high resolution structured light scanning, Int. Arch. Photogramm. Remote Sens. Spat. Inf. Sci. - ISPRS Arch. (2019) 965–972, https://doi.org/10.5194/isprs-archives-XLII-2-W15-965-2019.

[15] P. Targowski, M. Góra, M. Wojtkowski, Optical coherence tomography for artwork diagnostics, Laser Chem. 2006 (2006) 1–11, https://doi.org/10.1155/2006/35373, 35373.

[16] H. Liang, M.G. Cid, R.G. Cucu, G.M. Dobre, A.G. Podoleanu, J. Pedro, D. Saunders, En-face optical coherence tomography - a novel application of non-invasive imaging to art conservation, Opt Express 13 (2005) 6133, https://doi.org/10.1364/opex.13.006133.

[17] N. Proietti, D. Capitani, V. Di Tullio, Applications of nuclear magnetic resonance sensors to cultural heritage, Sensors 14 (2014) 6977–6997, https://doi.org/10.3390/s140406977.

[18] G. Filippidis, M. Massaouti, A. Selimis, E.J. Gualda, J.M. Manceau, S. Tzortzakis, Nonlinear imagig and THz diagnostic tools in the service of cultural heritage, Appl. Phys. Mater. Sci. Process 106 (2012) 257–263, https://doi.org/10.1007/s00339-011-6691-7.

[19] D. Anglos, Laser-induced breakdown spectroscopy in art and archaeology, Appl. Spectrosc. 55 (2001) 186A–205A. https://www.osapublishing.org/abstract.cfm?uri=as-55-6-186A.

[20] D. Anglos, V. Detalle, Cultural heritage applications of LIBS, in: Springer Ser. Opt. Sci., Springer Verlag, 2014, pp. 531–554, https://doi.org/10.1007/978-3-642-45085-3_20.

[21] A. Nevin, G. Spoto, D. Anglos, Laser spectroscopies for elemental and molecular analysis in art and archaeology, Appl. Phys. Mater. Sci. Process 106 (2012) 339–361, https://doi.org/10.1007/s00339-011-6699-z.
[22] E. Tognoni, V. Palleschi, M. Corsi, G. Cristoforetti, Quantitative micro-analysis by laser-induced breakdown spectroscopy: a review of the experimental approaches, Spectrochim. Acta-Part B At. Spectrosc. 57 (2002) 1115–1130, https://doi.org/10.1016/S0584-8547(02)00053-8.
[23] K. Melessanaki, M. Mateo, S.C. Ferrence, P.P. Betancourt, D. Anglos, The application of LIBS for the analysis of archaeological ceramic and metal artifacts, Appl. Surf. Sci. 197–198 (2002) 156–163, https://doi.org/10.1016/S0169-4332(02)00459-2.
[24] A. Giakoumaki, K. Melessanaki, D. Anglos, Laser-induced breakdown spectroscopy (LIBS) in archaeological science-applications and prospects, Anal. Bioanal. Chem. 387 (2007) 749–760, https://doi.org/10.1007/s00216-006-0908-1.
[25] M. Oujja, M. Sanz, F. Agua, J.F. Conde, M. García-Heras, A. Dávila, P. Oñate, J. Sanguino, J.R. Vázquez De Aldana, P. Moreno, M.A. Villegas, M. Castillejo, Multianalytical characterization of Late Roman glasses including nanosecond and femtosecond laser induced breakdown spectroscopy, J. Anal. At. Spectrom. 30 (2015) 1590–1599, https://doi.org/10.1039/c5ja00150a.
[26] A. Martínez-Hernández, M. Oujja, M. Sanz, E. Carrasco, V. Detalle, M. Castillejo, Analysis of heritage stones and model wall paintings by pulsed laser excitation of Raman, laser-induced fluorescence and laser-induced breakdown spectroscopy signals with a hybrid system, J. Cult. Herit. 32 (2018) 1–8, https://doi.org/10.1016/j.culher.2018.02.004.
[27] X. Bai, D. Syvilay, N. Wilkie-Chancellier, A. Texier, L. Martinez, S. Serfaty, D. Martos-Levif, V. Detalle, Influence of ns-laser wavelength in laser-induced breakdown spectroscopy for discrimination of painting techniques, Spectrochim. Acta Part B At. Spectrosc. 134 (2017) 81–90, https://doi.org/10.1016/j.sab.2017.06.008.
[28] K. Muller, H. Stege, Evaluation of the analytical potential of laser-induced breakdown spectrometry (LIBS) for the analysis of historical glasses, Archaeometry 45 (2003) 421–433, https://doi.org/10.1111/1475-4754.00119.
[29] N. Carmona, M. Oujja, S. Gaspard, M. García-Heras, M.A. Villegas, M. Castillejo, Lead determination in glasses by laser-induced breakdown spectroscopy, Spectrochim. Acta Part B At. Spectrosc. 62 (2007) 94–100, https://doi.org/10.1016/j.sab.2007.01.003.
[30] N. Carmona, M. Oujja, E. Rebollar, H. Römich, M. Castillejo, Analysis of corroded glasses by laser induced breakdown spectroscopy, Spectrochim. Acta Part B At. Spectrosc. 60 (2005) 1155–1162, https://doi.org/10.1016/j.sab.2005.05.016.
[31] T. Palomar, M. Oujja, M. García-Heras, M.A. Villegas, M. Castillejo, Laser induced breakdown spectroscopy for analysis and characterization of degradation pathologies of Roman glasses, Spectrochim. Acta Part B At. Spectrosc. 87 (2013) 114–120, https://doi.org/10.1016/j.sab.2013.05.004.
[32] S. Klein, T. Stratoudaki, V. Zafiropulos, J. Hildenhagen, K. Dickmann, T. Lehmkuhl, Laser-induced breakdown spectroscopy for on-line control of laser cleaning of sandstone and stained glass, Appl, Phys. A Mater. Sci. Process. 69 (1999) 441–444, https://doi.org/10.1007/s003390051029.
[33] C. Gerhard, J. Hermann, L. Mercadier, L. Loewenthal, E. Axente, C.R. Luculescu, T. Sarnet, M. Sentis, W. Viöl, Quantitative analyses of glass via laser-induced breakdown spectroscopy in argon, Spectrochim. Acta Part B At. Spectrosc. 101 (2014) 32–45, https://doi.org/10.1016/j.sab.2014.07.014.
[34] E. Negre, V. Motto-Ros, F. Pelascini, S. Lauper, D. Denis, J. Yu, On the performance of laser-induced breakdown spectroscopy for quantitative analysis of minor and trace elements in glass, J. Anal. At. Spectrom. 30 (2015) 417–425, https://doi.org/10.1039/c4ja00363b.
[35] A. Romani, C. Clementi, C. Miliani, G. Favaro, Fluorescence spectroscopy: a powerful technique for the noninvasive characterization of artwork, Acc. Chem. Res. 43 (2010) 837–846, https://doi.org/10.1021/ar900291y.
[36] B.J. Bozlee, A.K. Misra, S.K. Sharma, M. Ingram, Remote Raman and fluorescence studies of mineral samples, Spectrochim. Acta Part A Mol. Biomol. Spectrosc. 61 (2005) 2342–2348, https://doi.org/10.1016/j.saa.2005.02.033.
[37] D. Ehrt, Photoactive glasses and glass ceramics, IOP Conf. Ser. Mater. Sci. Eng. 21 (2011), 012001, https://doi.org/10.1088/1757-899X/21/1/012001.
[38] D. Ehrt, Photoluminescence in glasses and glass ceramics, in: IOP Conf. Ser. Mater. Sci. Eng., IOP Publishing, 2009, 12001, https://doi.org/10.1088/1757-899X/2/1/012001.
[39] J. Fournier, J. Néauport, P. Grua, V. Jubera, E. Fargin, D. Talaga, S. Jouannigot, Luminescence study of defects in silica glasses under near-UV excitation, in: Phys. Procedia, Elsevier B.V., 2010, pp. 39–43, https://doi.org/10.1016/j.phpro.2010.10.009.
[40] R. Reisfeld, L. Boehm, B. Barnett, Luminescence and nonradiative relaxation of Pb2+, Sn2+, Sb3+, and Bi3+ in oxide glasses, J. Solid State Chem. 15 (1975) 140–150, https://doi.org/10.1016/0022-4596(75)90237-6.
[41] L. Skuja, Section 1. Defect studies in vitreous silica and related materials: optically active oxygen-deficiency-related centers in amorphous silicon dioxide, J. Alloys Compd. 239 (1998) 16–48, https://doi.org/10.1016/0925-8388(96)02241-4.
[42] R. Reisfeld, Inorganic ions in glasses and polycrystalline pellets as fluorescence standard reference materials, J Res Nat Bur Stand Sect A Phys Chem 76 (1972) 613–635, https://doi.org/10.6028/jres.076A.054.
[43] G. Filippidis, G.J. Tserevelakis, A. Selimis, C. Fotakis, Nonlinear imaging techniques as non-destructive, high-resolution diagnostic tools for cultural heritage studies, Appl. Phys. Mater. Sci. Process 118 (2014) 417–423, https://doi.org/10.1007/s00339-014-8357-8.
[44] M. Oujja, S. Psilodimitrakopoulos, E. Carrasco, M. Sanz, A. Philippidis, A. Selimis, P. Pouli, G. Filippidis, M. Castillejo, Nonlinear imaging microscopy for assessing structural and photochemical modifications upon laser removal of dammar varnish on photosensitive substrates, Phys. Chem. Chem. Phys. 19 (2017) 22836–22843, https://doi.org/10.1039/c7cp02509b.
[45] T.E. Villafana, W.P. Brown, J.K. Delaney, M. Palmer, W.S. Warren, M.C. Fischer, Femtosecond pump-probe microscopy generates virtual cross-sections in historic artwork, Proc. Natl. Acad. Sci. U.S.A. 111 (2014) 1708–1713, https://doi.org/10.1073/pnas.1317230111.
[46] A. Dal Fovo, M. Sanz, S. Mattana, M. Oujja, M. Marchetti, F.S. Pavone, R. Cicchi, R. Fontana, M. Castillejo, Safe limits for the application of nonlinear optical microscopies to cultural heritage: a new method for in-situ assessment, Microchem. J. 154 (2020) 104568, https://doi.org/10.1016/j.microc.2019.104568.
[47] A. Dal Fovo, M. Sanz, M. Oujja, R. Fontana, S. Mattana, R. Cicchi, P. Targowski, M. Sylwestrzak, A. Romani, C. Grazia, G. Filippidis, S. Psilodimitrakopoulos, A. Lemonis, M. Castillejo, In-depth analysis of egg-tempera paint layers by multiphoton excitation fluorescence microscopy, Sustainability 12 (2020) 3831, https://doi.org/10.3390/su12093831.
[48] H. Liang, M. Mari, C.S. Cheung, S. Kogou, P. Johnson, G. Filippidis, Optical coherence tomography and non-linear microscopy for paintings – a study of the complementary capabilities and laser degradation effects, Opt Express 25 (2017) 19640, https://doi.org/10.1364/oe.25.019640.
[49] G. Latour, J.-P. Echard, M. Didier, M.-C. Schanne-Klein, In situ 3D characterization of historical coatings and wood using multimodal nonlinear optical microscopy, Opt Express 20 (2012) 24623, https://doi.org/10.1364/oe.20.024623.
[50] Y.-C. Chen, H.-C. Hsu, C.-M. Lee, C.-K. Sun, Third-harmonic generation susceptibility spectroscopy in free fatty acids, J. Biomed. Opt. 20 (2015), 095013, https://doi.org/10.1117/1.jbo.20.9.095013.
[51] T. Palomar, F. Agua, M. García-Heras, M.A. Villegas, Chemical degradation and chromophores of 18th century window glasses, Glas. Technol. - Eur. J. Glas. Sci. Technol. Part A. 52 (2011) 145–153. https://www.ingentaconnect.com/content/sgt/gta/2011/00000052/00000005/art00001.
[52] M. García-Heras, M.A. Villegas, Vidrieras de la Catedral de León, Geomaterials 2 Project, Regional Government of Madrid, 2018. https://www.secv.es/libro-vidrieras-de-la-catedral-de-leon-arqueometria-de-materiales/.
[53] A. Dal Fovo, M. Oujja, M. Sanz, A. Martínez-Hernández, M.V. Cañamares, M. Castillejo, R. Fontana, Multianalytical non-invasive characterization of phthalocyanine acrylic paints through spectroscopic and non-linear optical techniques, Spectrochim. Acta Part A Mol. Biomol. Spectrosc. 208 (2019) 262–270, https://doi.org/10.1016/j.saa.2018.09.040.
[54] NIST atomic spectra database online at (n.d.), https://physics.nist.gov/PhysRefData/ASD/lines_form.html.
[55] P.C. Schultz, Optical absorption of the transition elements in vitreous silica, J. Am. Ceram. Soc. 57 (1974) 309–313, https://doi.org/10.1111/j.1151-2916.1974.tb10908.x.
[56] R. Reisfeld, N. Lieblich, Absorption and fluorescence of lead in germanate, borate and phosphate glasses, J. Non-Cryst. Solids 12 (1973) 207–212, https://doi.org/10.1016/0022-3093(73)90070-7.
[57] R.W.B. Pearse, A.G. Gaydon, The Identification of Molecular Spectra, third ed., n.d, Chapman and Hall Ltd, London, 1963 https://doi.org/10.1038/148240a0.
[58] G.W. White, Improving the accuracy of vertical measurements under the microscope, Microscope 18 (1970) 51–59. http://www.microscopy-uk.org.uk/mag/indexmag.html?http://www.microscopy-uk.org.uk/mag/artjun05/gothicknes s.html.
[59] Refractive index of METALS - lead (n.d.), https://refractiveindex.info/?shelf=3d&book=metals&page=lead.
[60] M. Mari, G. Filippidis, Non-linear microscopy: a well-established technique for biological applications towards serving as a diagnostic tool for in situ cultural heritage studies, Sustainability 12 (2020), https://doi.org/10.3390/su12041409, 1409.